Suplemento de la Revista Mexicana de Física **1** (3) 9–16 JULY–AUGUST 2020

Optical metrology beyond Abbe and Rayleigh

J. Bischoff[a,*], R. Mastylo[a], G. Granet[b], and E. Manske[a]
[a] *Institute for Process Metrology, Technical University of Ilmenau, 98684 Ilmenau, Germany.*
[b] *Université Clermont Auvergne, CNRS, SIGMA Clermont, Institut Pascal, F-63000 Clermont-Ferrand, France.*
[*] *e-mail: joerg.bischoff@tu-ilmenau.de*
phone +49 3677 695055

Received 6 September 2019; accepted 12 November 2019

For many years, it was believed that optical microscopy and metrology was limited in resolution related to the light wavelength as suggested by Ernst Abbe and Lord Rayleigh. In the recent past, several approaches have been developed to overcome these limitations such as the Nobel prize honored STED or optical CD as widely used in the semiconductor metrology. Unfortunately, both techniques need special samples. While STED relies on fluorescence, OCD requires grating samples. In our contribution, we present two model-based (mb) approaches to overcome some of these restrictions. One is mb Laser Focus Scanning (mLFS). Here, we show how to improve the accuracy of edge detection from several hundred nm to about 10-20 nm by exploiting rigorous modeling. The second one is Scanning Coherent Fourier Scatterometry (SCFS) where the diffracted Fourier spectrum is detected, and the attempt is undertaken to retrieve the sample profile. It is shown that this technique is very sensitive, particularly when the phase is recorded by means of a wave-front sensor. Measurements and simulations for periodic, as well as for aperiodic sub-resolution features, show already good agreement. Moreover, we strongly believe that the observed high sensitivity of the Fourier spectra opens the path to quantitatively measurements below the resolution limits of light.

Keywords: Optical profilometry; diffraction modeling; surface metrology

1. Introduction

For many years, optical microscopy and metrology was limited by resolution constraints related to the light wavelength as suggested by Ernst Abbe and Lord Rayleigh. Recently, several approaches have been developed to overcome these limitations. On the one hand, Nobel laureate Hell proposed to tailor the Airy disc by means of special beam profiles of two consecutive laser pulses in order to achieve smaller spot sizes resulting in super-resolution [1]. Unfortunately, his method requires two stable energy states such as fluorescence. A quite different method-called scatterometry or optical CD (OCD) is applied in semiconductor metrology [2,3]. Here, the spectral fingerprint of periodic test patterns is recorded, and the causing profile is then reconstructed by means of rigorous diffraction solvers in combination with inverse methods. Since only the specular reflected light (*i.e.*, the zeroth diffraction order) is exploited, another way was opened to circumvent the Abbe condition of having at least two orders to interfere to form an image pattern. Therefore, patterns with periods of as little as 20 nm can be measured with Angstrom accuracy by using spectral ranges from UV through VIS. The disadvantages of this approach are that it requires grating structures and a-priori knowledge about the measurement sample. In this paper, we present a model-based approach that is shown to be able to overcome these restrictions. In our approach, the diffraction that occurs when an optical beam hits a topographic sample is modeled by rigorous modal diffraction methods such as RCWA and C-method. In addition, we are using ray tracing to model the classical optical imaging. In order to demonstrate the potential of the method, we have applied the method to two challenges of today's optical metrology-determining the position of profile edges with accuracy well below the diffraction blur and measuring aperiodic features below the classical diffraction limit.

2. Measurement hardware

The principal schemas of our measurement arrangements are presented in Fig. 1. On the left hand side, the Laser Focus Scanning (LFS) in a confocal arrangement is shown. Alternatively, an astigmatic objective lens or a Foucault knife setup can be utilized as defocusing sensor [4,5].

The right hand side shows the basic principle of the Coherent Fourier Transform Scatterometry (CFS) [6]. Both setups are almost identical. However, in LFS the beam is refocused onto the detector to derive a signal for the defocusing. More detailed descriptions of this technique can be found in previous publications of our group [4,5,7]. In contrast, the CFS

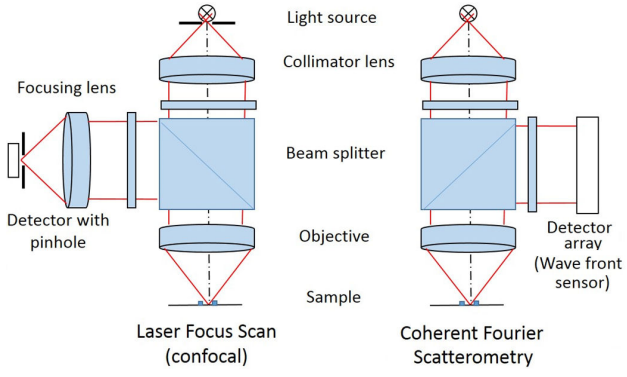

FIGURE 1. Left hand side: Basic principle of Laser Focus Scanning. Right hand side: Coherent Fourier Scatterometry.

measures the angular diffraction spectrum, and thus can avoid the refocus. Actually, there are two principal options to measure the angular distribution of the diffracted light in CFS. On the one hand, the intensity can be recorded by just putting a regular detector array such as a CCD or a CMOS camera (only the chip). On the other hand, it is possible to measure the phase of the diffracted wave-front by means of some kind of wave-front sensor. To this end, we applied a Shack Hartmann sensor (SHS) from Optocraft [8]. However, other kind of wave-front sensors such as interferometric setups have also been reported for use in CFS [9]. A measuring unit was developed and built based on a commercial DVD pickup. It was attached to the nano-positioning and measuring machine (NPMM) of the Institute for Process Metrology of TU Ilmenau. This machine allows measurement volumes of 200×200 square millimeters and beyond with nano-meter positioning accuracy [10]. It has to be stressed that we are using a scanning CFS (SCFS) as opposed to the CFS-setups suggested in previous publications. In this way, we are not restricted to grating samples.

3. Modeling

An accurate modeling is key to overcome limitations due to diffraction. Therefore, the next section is devoted to this topic. A detailed description of the LFS model is given already in a previous paper [7]. Thus, only a short summary of our LFS modeling shall be given here. Basically, the model is a combination of ray-tracing with sophisticated modal diffraction theory. In our model, the rays carry both phase and polarization. The ray tracing is applied everywhere to follow the propagating light from the source all the way to the sample. There, the interaction of the incident beam with the sample is determined by diffraction. For this reason, a sophisticated diffraction solver has to be applied here to maintain the overall accuracy of the model. We employ an algorithm that is based on the Rigorous Coupled Wave Approach (RCWA) [11,12] also known as Fourier Modal Method [13]. Alternatively, we have implemented another approach that is based on Chandezon's coordinate transformation method [14]. Both methods can be nicely combined into the same S-matrix framework [15]. For our simulations, we have used the commercial package UNIGIT [16]. Directly derived from Maxwell's equations, the algorithm fully incorporates the vectorial character of electromagnetic waves including polarization. It is based on the idea, that an isolated or single feature can be treated by means of a modal method by embedding it into a sort of super-period [17,18]. Using the periodic continuation, the pitch-to-wavelength ratio determines the angular resolution of the scattering as well as the angular sampling of the incident wave. It was shown in [18] that the resulting diffraction distribution converges with increasing pitch. The application of perfect matched layers (PML) helps to accelerate the convergence.

In principle, a full 3D approach would be required to keep up with real measurement. Consequently, a crossed gratings RCWA should be employed [19]. However, the embedding into a larger super-period results inevitably in large truncation numbers M of at least ±30 for one spatial direction. This quickly leads to non-acceptable computation times or even exceeds the capabilities of available computation hardware. Therefore, a so-called 2.5 dimensional approach was developed for the modeling of two-dimensional (line-space) profiles. The key idea behind the 2.5D model is to use full 3D propagation of the rays while modeling the diffraction only two-dimensionally. To this end, sections through the pupil are taken, and a conical diffraction solver [20] is applied to each section. The according pupil discretization schema is shown in Fig. 2. The plane waves of the incident beam in the pupil plane are described by two parameters: the polar angle of incidence (AOI) θ_i after focusing, and the azimuthal AOI φ_i. They can be directly connected to the ray-tracing of the remaining optical model. The pupil is sampled employing equidistant lines parallel to the main tangential plane indicated as solid (green) lines. The directions of the main tangential plane and the sampling lines have to be parallel to the scanning direction, which itself is orthogonal to the lines, edges, and trenches of the surface profile (as indicated by red dashed lines). Each sampling line is determined by $\varphi_i = 90^\circ$, and $\theta_i = n \cdot /p$ where λ is the wavelength of the incident light, p the period, and n is an integer between $\pm N$ ($N = NA \cdot p/\lambda$). All diffraction orders (located at the crossovers of the green lines with the red dashed lines) of the respective line remain on this line. The period-to-wavelength-ratio determines the ray sampling in the angular (k) space.

Usually, the polarization components of the diffracted (outgoing) fields in reflection are obtained from the incident polarization components in Jones notation by:

$$\begin{pmatrix} \mathbf{A}_s^0 \\ \mathbf{A}_p^0 \end{pmatrix} = \begin{pmatrix} \mathbf{r}_{ss} & \mathbf{r}_{ps} \\ \mathbf{r}_{sp} & \mathbf{r}_{pp} \end{pmatrix} \cdot \begin{pmatrix} \mathbf{A}_s^i \\ \mathbf{A}_p^i \end{pmatrix} = \mathbf{R} \cdot \begin{pmatrix} \mathbf{A}_s^i \\ \mathbf{A}_p^i \end{pmatrix}. \quad (1)$$

Here, the $\mathbf{r}_{ij}$ represent fully populated sub-matrices. The matrix size is determined by the truncation number. A full diffraction matrix $\mathbf{R}$ according to (1) is computed for each sampling line in Fig. 2. Then, the full diffraction matrix of the 3D system is assembled from all conical sections and multiplied with the matrix of the complex amplitude distribution of the incident beam. This corresponds to a convolution in real space. Details of how to assemble the full diffraction matrix and how to sample the incident beam are given in [7]. Eventually, a full matrix comprising all outgoing modes (or plane waves) results. Moreover, known aberrations of the optical system whether intended or not (*e.g.*, an astigmatic term), pupil effects and intensity profiles (*e.g.* Gaussian beam) can be applied by means of filter functions.

Finally, the intensity distribution on the detector diode has to be calculated and a height signal has to be derived. The detector area is discretized and the ray fixed E-field components (p, s, r) have to be transformed into a detector fixed system (x, y, z). This is achieved by means of a transformation matrix $\mathbf{T}$:

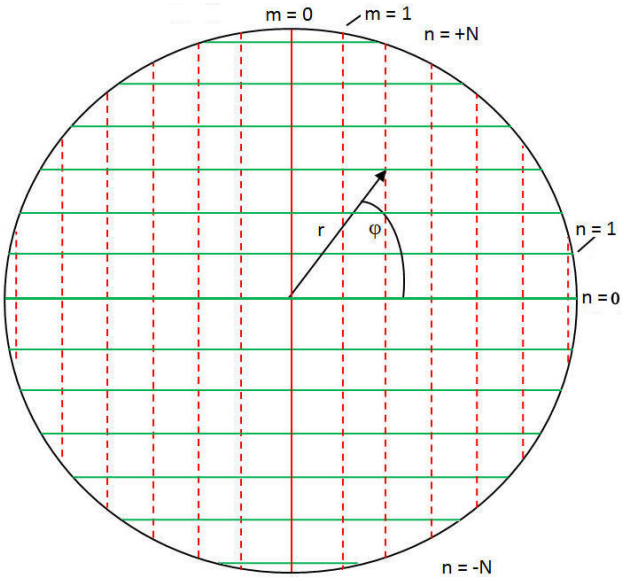

FIGURE 2. Pupil sampling for 2.5D model.

$$\begin{pmatrix} A_x \\ A_y \\ A_z \end{pmatrix} = \mathbf{T} \cdot \begin{pmatrix} A_p \\ A_s \\ A_r \end{pmatrix} \quad \text{with}$$

$$\mathbf{T} = \begin{pmatrix} \cos\varphi \cdot \cos\theta & \sin\varphi \cdot \cos\theta & -\sin\theta \\ -\sin\varphi & \cos\varphi & 0 \\ \cos\varphi \cdot \sin\theta & \sin\varphi \cdot \sin\theta & \cos\theta \end{pmatrix}. \quad (2)$$

Besides, the scanning motion is simulated by multiplying the incident plane wave spectrum by additional phase terms for the lateral positions x and y, and the vertical position z:

$$A_{I,mn}(x,y) = A_{I,mn}(0,0) \cdot \exp\left(i\frac{2\pi}{\lambda} \cdot \beta_{x,m} \cdot x\right)$$
$$\times \exp\left(i\frac{2\pi}{\lambda} \cdot \beta_{y,n} \cdot y\right) \cdot \exp\left(-i\frac{2\pi}{\lambda} \cdot \alpha_{mn} \cdot z\right). \quad (3)$$

Here, the lateral wave vector components β_{xn} and β_{yn} are given by: $\beta_(x,m) = \beta_(x,0) + m(\lambda/p)$ and $\beta_{y,n} = \beta_{y,0} + n(\lambda/p)$ while the vertical wave vector component of the mode $(m,n)\alpha_{mn}$ follows from the dispersion relation:

$$\alpha_{mn} = \sqrt{1 - \beta_{x,m}^2 - \beta_{y,n}^2}. \quad (4)$$

Equation (3) also includes a vertical offset z, which is of course very useful to model the focusing of the sensor. Since the diffraction computation and the illumination/detection paths are completely decoupled, only one time-consuming diffraction solving is required for a certain profile. The resulting diffraction matrix can be stored and reused for different detection and scanning schemas. This greatly reliefs the computation resource issues. The modeling of the different focal sensor principles fits also very well into this schema (*e.g.*, an astigmatic sensor can be modeled quite straightforward by means of a phase filter in the collimated beam). Concurrently, known rest aberrations of the optics could be likewise taken into consideration. In addition, the intensity distribution (see above) on the detector has to be evaluated by means of a quadrant diode which is oriented either by 45° or 0○ degrees relative to the grating lines. Similar approaches have been implemented for the Foucault and the pin-hole sensor.

Due to the high degree of similarity of both methods, the modeling of the CFS metrology proceeds along the same lines as stated above for the LFS. The crucial difference is that the diffracted wave-front is not refocused anymore but directly propagated to the detector. In terms of modeling, it means that we can abstain from the transformation and superposition which is symbolized by Eq. (2). Instead, either the intensity or the phase of all diffracted plane waves, which are collected by the NA of the objective lens, has to be calculated resulting in $I(\theta,\varphi)$ or $\Delta(\theta,\varphi)$, respectively. Again, the strongly focused beam is scanned across the sample and one finally obtains an intensity or phase distribution for all scanning positions x or (x,y), respectively.

Both model-based metrology techniques have in common that an inverse problem has to be solved in order to retrieve an unknown profile from a measured signal. Although, the signal is by far more complex in CFS (one value per order and scan position) as compared to LFS (usually just one value per scan position). For the inversion, a variety of methods is known in the metrology community. We have implemented two search methods: one local approach, the Levenberg-Marquardt Approach (LMA) [21], and one global approach, the Particle Swarm Optimization (PSO) [22]. Usually, first a PSO is run to provide a good start solution for a consecutive LMA-run. Some first results on the profile reconstruction from LFS measurements can be found in [23].

4. Experimental and results

In this section, we are going to present some first measurements and discuss the profile reconstruction by means of the inverse methods. The first part is treating the LFS method.

4.1. Laser focus scanning

The main goal was to improve the lateral accuracy of edge detection by means of sophisticated modeling. Moreover, we are aiming at a complete edge shape reconstruction, *i.e.*, to include additional edge features such as side wall angle and corner rounding. The basic challenge of this metrology task is depicted in Fig. 3. In “standard” metrology, the edge position is supposed to be located at 50% signal height. Obviously, an error of several hundred nanometer would result in the worst case. Even worse, the observed delta also depends on step height, material and polarization.

Some important results are published already in [7]. The first one is the measurement of a step being approximately 80 nm in height etched in Al. The fit of the simulated signal

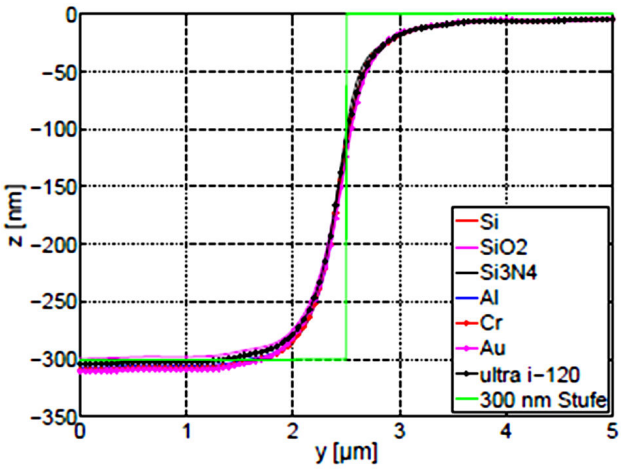

FIGURE 3. LFS signal vs. edge location for a 300 nm step (various materials).

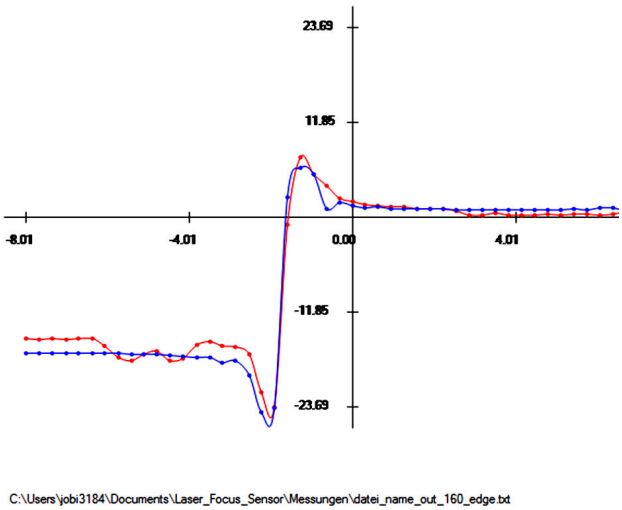

FIGURE 4. LFS measurement signal vs. simulated signal for a 160 nm Al step.

to the measured signal was presented in Fig. 9 in [7]. The match match is not ideal, however, it shows already a good qualitative agreement. As pointed out in the previous publication, the main contribution might be the rotation of the signal due to a slight tilt in the scan direction. A step height of 84 nm (confirmed by an AFM measurement), and an edge position delta of about 400 nm relative to the assumed location resulted from the inversion. In the second example, a nominal step height of 160 nm was chosen. As can be seen in Fig. 4, the fit is quite good. Furthermore, the edges almost coincide.

Therefore, we dare to claim that the edge position can be determined within 10 to 20 nm accuracy through our model-based LFS approach. The remaining misfit between the signals has to be very likely attributed to the fact that the measured profile is far from being ideal as assumed in the simulation. Quite the contrary, a scanning electron micrograph (SEM) revealed granularity and some kind of waviness across the profile slope (compare Fig. 5) which could also be

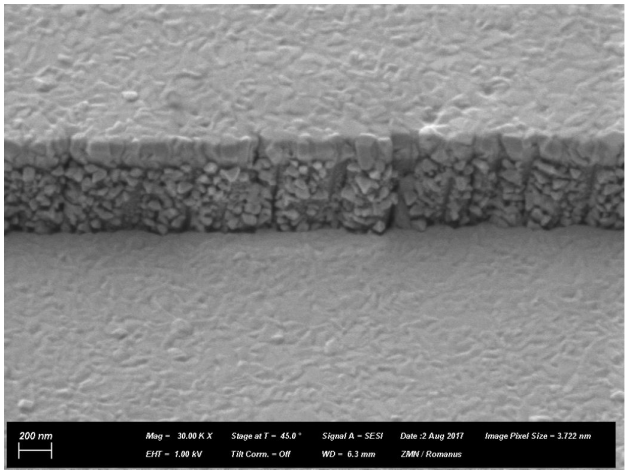

FIGURE 5. Scanning electron micrograph of the LFS sample.

confirmed by the AFM measurements. Besides, the Al coating did not cover the slope as intended (the material boundary can be clearly identified in the SEM figure). Unfortunately, our current code does not allow to model the subtleties in the profile as revealed by the SEM picture. In order to address the granularity and waviness adequately, a crossed grating diffraction solver has to be used rather than the line-space solver as discussed for the 2.5D model in section 3. Therefore, we are planning first to repeat the measurement and inversion procedure with a more ideal binary sample profile in the next step.

LFS itself is in principal limited by the Rayleigh resolution criterion or Abbe criterion, respectively for gratings. This means that two features closely below this limit cannot be resolved and thus not be measured by LFS. This could be also confirmed by another numerical investigation related to LFS [24]. However, the resolution issue could also be overcome by recording the Fourier spectrum reflected and diffracted from the sample by means of a detector array as suggested in Fourier scatterometry [6] rather than deriving a height signal such as in standard LFS. Some first experimental attempts in this direction shall be discussed in the next subsection.

4.2. Scanning coherent Fourier transform scatterometry

As shown in Fig. 1, the experimental setup for SCFS requires only a slight modification of the LFS setup. Actually, the detector focusing lens has to be removed, and the (quadrant) diode detector is replaced either by a detector array to measure the angular intensity spectrum or by some kind of wave-front sensor such as a Shack-Hartmann sensor to measure the phase of the diffracted wave-front.

In order to show that SCFS has the ability to overcome, both the Abbe as well as the Rayleigh resolution criterion, we investigated to kind of sample patterns-periodic gratings with sub-resolution pitch as well as specially prepared aperiodic features. Periodic grating measurements have been per-

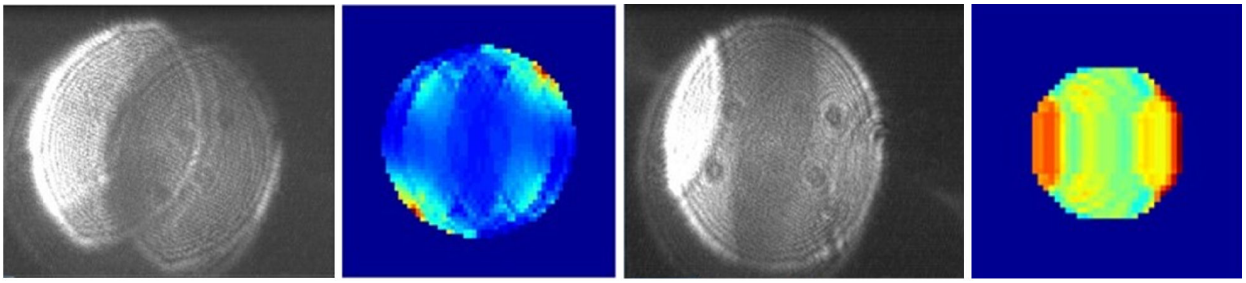

FIGURE 6. CFS intensity spectra of Si-gratings recorded with a $NA = 0.55$ lens @650 nm (from left to right: a) pitch = 2 μm measurement, b) pitch = 2 μm simulation, c) pitch = 0.8 μm measurement, d) pitch = 0.8 μm simulation).

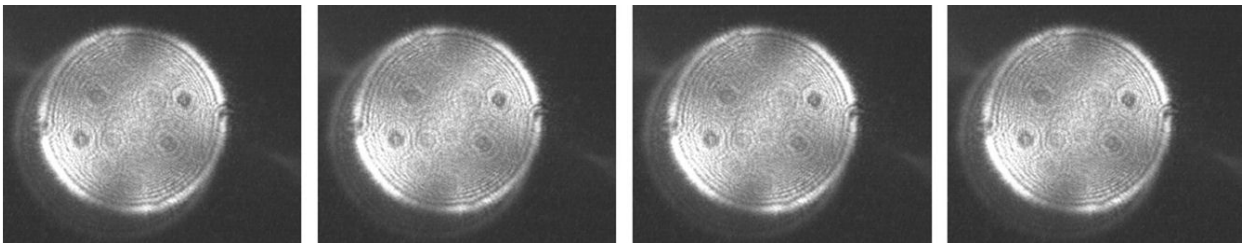

FIGURE 7. CFS intensity spectra for a 0.4 μm pitch Si L/S grating (recorded with $NA = 0.55$ lens @650 nm) 4 consecutive scan locations.

formed on a Simetric's AFM resolution standard RS-N [25]. It comprises 9 gratings with pitches from 0.4 microns through 6 microns. All gratings possess equal line and space width. The nominal etching depth is 190 nm. When recording the Fourier image by means of a camera array, a movie clearly reveals the high sensitivity of the signal on slightest position and profile changes while scanning laterally across the grating samples. Furthermore, the comparisons of the simulated Fourier distributions with measurements show qualitative and quantitative agreements from good to very good. Two examples of CFS intensity measurements vs. simulations are shown below. In both cases, the NA of the focusing lens was 0.55 and the measurement wavelength was 650 nm. The first example in Fig. 6 shows the Fourier distribution patterns as recorded from a line space grating etched in Si with pitch = 2 microns (a measurement, and b simulation). It can clearly be seen that due to the smaller wavelength-pitch ratio the two first diffraction orders overlap considerably. Moreover, a good qualitative and quantitative agreement between simulation and measurement could be achieved with little effort (aside from a slight rotation in the experiment). The second example in Fig. 6 compares a measured Fourier spectrum with a simulation for a 0.8 μm pitch grating. Obviously, the two first diffraction orders are not overlapping anymore but move away from each other.

Apparently, the gratings considered in Fig. 6 possess a pitch above or short below the Abbe limit (normal incidence) of $\lambda/NA = 0.65$ nm$/0.55 = 1.18$ μm. This means that the center of the first orders are within the receiving pupil circle for the 2 μm grating while for the 0.8 μm pitch grating only a small region of the first order wave can be captured by the pupil. Furthermore, the intensity spectra exhibit clear differences while scanning across the grating (pictures are not shown here).

Hence, we investigated an even more extreme case of a grating with 0.4 μm pitch. Figure 7 exhibits the measured intensity distributions for four consecutive scan positions (cut out of a movie). Evidently, there is only very little change in the signal versus the scan positions. This change did not improve very much when the measurement was repeated with a Shack-Hartmann sensor to record the phase of the diffracted wave, rather than the intensity.

The preliminary conclusion here is that SCFS, just like the common CFS, shall be able to retrieve the average grating profile, such as from OCD, more or less without resolution limitations. However, the relative location of the probing beam w.r.t. the grating edges will be only detectable for gratings which are only slightly below the Abbe limit. Further tests are planned with sub-resolution gratings that are intentionally distorted to feature clear deviations between adjacent lines. Here, we expect more sensitivity relative to the scan position.

Due to the necessity of grating samples, the OCD lithographic metrology is forced to measure on reference patterns commonly placed on the scribe lane outside the chip area. Moreover, only averaged signals over many periods can be measured due to the large size of the spot. These limitations become more and more severe with shrinking feature sizes. Consequently, there has arisen a strong demand for independent measurements, which in turn require to abandon regular samples. This issue shall be addressed with our next example.

For this purpose, a special sample (called SRS-1) was prepared by means of ion-beam writing comprising a number of grating lines and spaces with different width (nominal widths are 100, 200, and 300 nm) etched into Silicon (see Fig. 8). The average etching depth is 50 nm. The real widths have been measured by means of SEM and are also shown

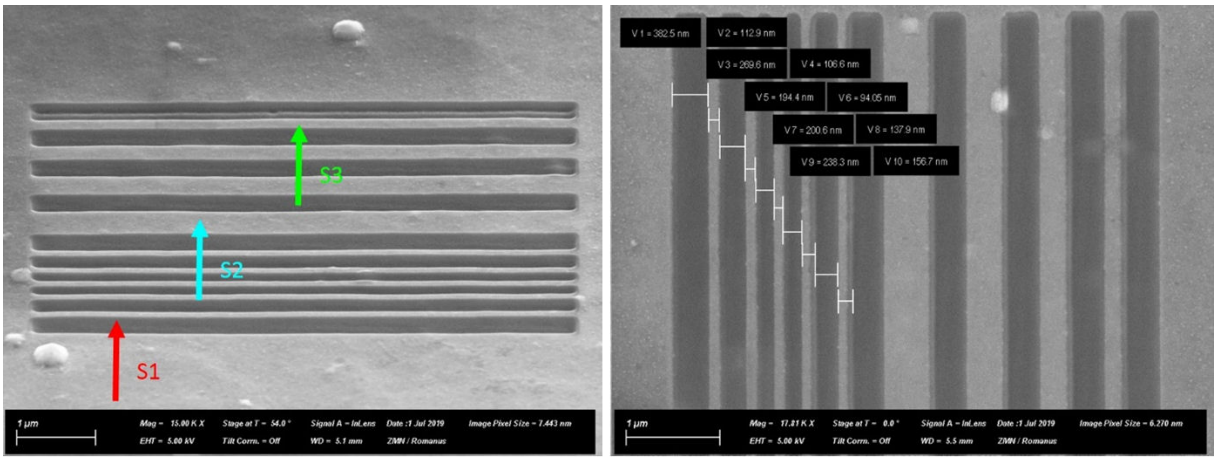

FIGURE 8. SEM micrographs of aperiodic test features etched in Si (nominal line and space widths are 100, 200, and 300 nm, respectively) called SRS-1 sample. Left hand side: oblique view. Right hand side: top view (rotated by 90 degrees).

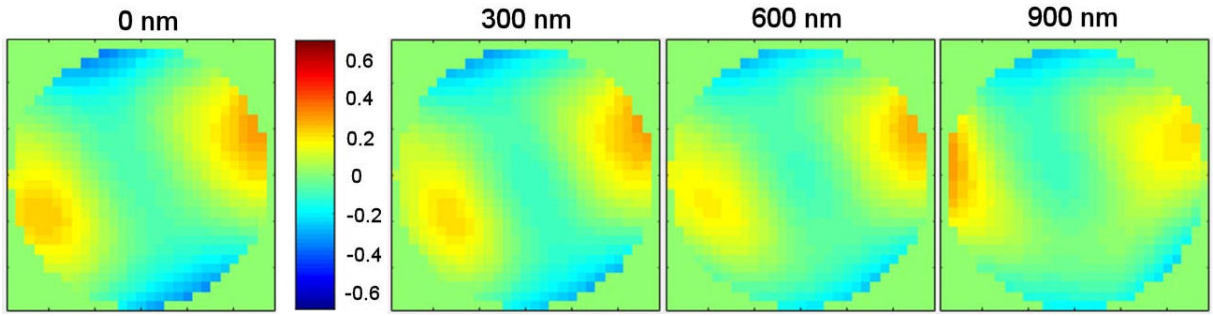

FIGURE 9. Measured CFS wave-front phase distributions for the SRS-1 sample at different scan positions indicated by arrow S1.

in the inlet of Fig. 8 (right hand side). The Rayleigh resolution limit for incoherent illumination is given by $\Delta x = 0.61(\lambda/NA)$ resulting in $\Delta x = 660$ nm (@$NA = 0.6$ and $\lambda = 650$ nm). Accordingly, all geometrical distances of our sample between adjacent lines or spaces, respectively are below this limit.

Firstly, CFS scans across the pattern have been done and the wave-front was recorded by means of the SHS. A step size of 100 nm for the lateral scan was chosen. Unfortunately, not all spectra can be shown due to the available space in the paper. The scan was started approximately 1 μm outside of the pattern. Accordingly, only little change can be seen there and the observed wave-front distortion is mainly caused by rest-aberrations of the optical system as well as some alignment issues (*e.g.* during positioning and setting the aperture cutout of the SHS).

On its further path, the beam interacts with the etched trenches and the wave-front starts to be getting more distorted (compare Fig. 10). At 2100 nm the wave-front warping becomes weaker again which is likely due to the reaching the first plateau near the arrow tip of S2.

Proceeding with the scan, the beam "sees" a few 300 nm trenches separated by plateaus of different width. The CFS phase spectra reflect this quite well. Particularly, phase fronts with strong warp (*e.g.* at 1500, 3700, and 4500 nm) alternate with smoother ones (*e.g.* at 2100, 3300, and 4100 nm). These observations correlate more or less with the geometry. Deviations might be attributed to deviations from the nominal widths as well to the different adjacent patterns on either side of the four broad lines (being 300 nm in nominal width). In addition, the nominal space width is reduced from trench to trench. However, more detailed investigations are necessary in order to be able to interpret the pupil figures correctly.

A modeling study may help to gain more insight. Moreover, accurate modeling is also required when the attempt is ventured to reconstruct the scanned profile from the pupil spectra. Our approach was as follows: First, we extracted the rest-aberrations from the outermost scan position (0 nm in Fig. 9) in terms of Zernike coefficients. Second, we plugged these values into the pupil filter function and modeled the diffracted wave-front occurring in the pupil when the profile of Fig. 8 would be probed by a laser beam with $NA = 0.6$, $\lambda = 650$ nm. Some first results are presented in Fig. 11. There is already some qualitative agreement to the experiment observable though an improved match is highly desirable in terms of quantitative metrology. It is suspected that the assumed rest-aberrations are erroneous. Furthermore, the measurements should be repeated at multiple lateral positions in order to average sample geometry variations and exclude artefacts. Besides, there are additional unknowns such as the exact etch depths (which also might vary).

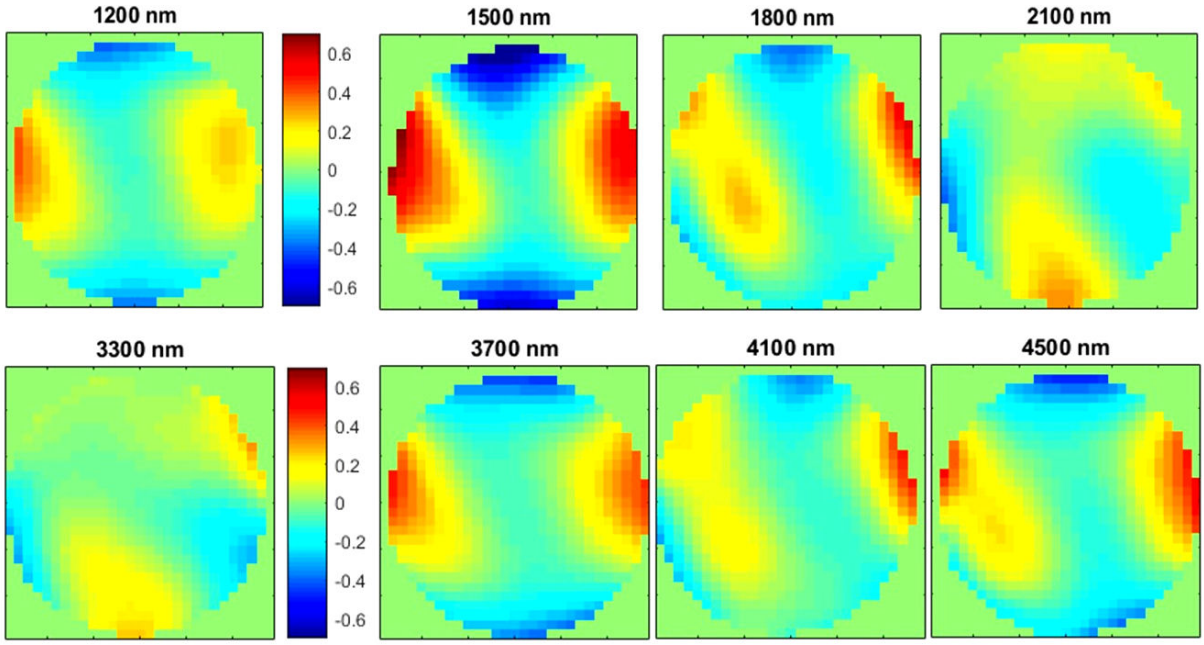

FIGURE 10. Measured CFS wave front phase distributions for the SRS-1 sample at different scan positions indicated by arrow S2 (top row) and arrow S3 (bottom row).

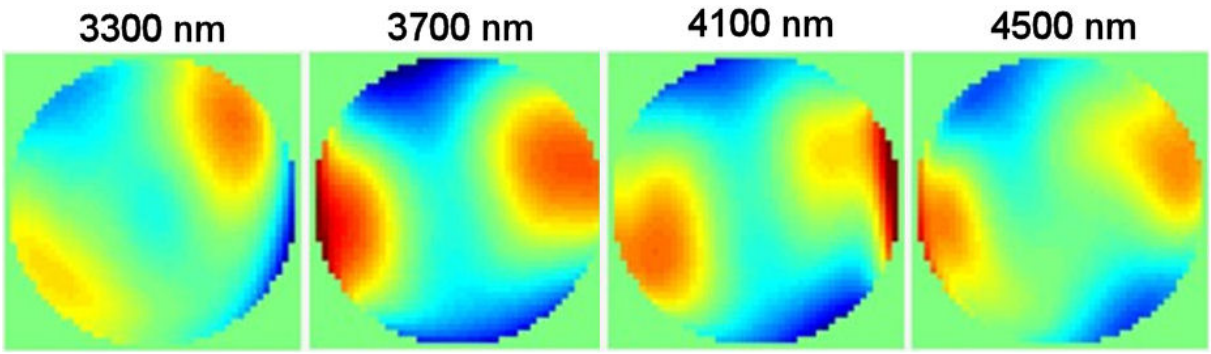

FIGURE 11. Simulated CFS wave front phase distributions for the sample shown in Fig. 8.

Profile reconstruction from the pupil images as shown above requires big efforts during the inversion. Therefore, data reduction would be desirable. A Zernike-decomposition is a widely used tool in optics and it comes for free with the SHS. In addition, an evaluation of the individual coefficients vs. the scan position may provide additional valuable insight into hidden relations. Figure 12 shows the third order and a few higher order Zernike coefficients vs. the scan position for a SCFS measurement of the SRS-1 sample. There are three coefficients that clearly show a strong dependency on the scanning position, namely the third order 0°: astigmatism term A22, the even third order coma term A31, and the odd three-foil term B33. Moreover, some kind of correlation with the profile is visible when comparing it with the inlet schematic cross section. However, it will require more research to discover the details.

5. Conclusions

A new modular optical metrology approach was presented that has the potential to overcome the classical resolution limits of Abbe and Rayleigh to some extent. It relies on model-based laser focus scanning (LFS) in combination with scanning Fourier transform scatterometry (SCFS). The feasibility of the method was shown by means of experiments. It could be proved that the new approach has the potential for super-resolution quantitative metrology of technical samples. This was demonstrated with three typical examples, the improvement of edge detection accuracy in LFS, CFS measurements on sub-resolution gratings, and SCFS measurements on aperiodic sub-resolution features. Particularly, we'd like to point out that scanning CFS is, to our knowledge, a new innovative approach that might be help to overcome the reference vs. in-die deviation issue in semiconductor industry.

Further work should be devoted to improve the correlation between measurement and modeling. To this end, the model has to be further developed to take more realistic sample properties such as roughness and more generic profile shapes (other than binary) into account. Moreover, the optical metrology hardware has to be analyzed more thoroughly and regarded in the model. For instance, the rest-aberrations play an important role especially in SCFS. It is planned to conduct further analysis and measurement to obtain more reliable values. In addition, the measurements shall be extended to other samples in order to gather better knowledge about the dependencies of the diffracted light in the pupil on the geometry illuminated by the micro-spot.

1. S. W. Hell, J. Wichmann, *Optics Letters* **19** (1994) 780-782.
2. X. Niu, N. Jakatdar, J. Bao and C.J. Spanos, *IEEE Trans. Semicond. Manufact*. **14** (2001) 97-111.
3. J. Bischoff, N. Jakatdar, X. Niu, *Proc. SPIE* (2003) 5038.
4. R. Mastylo, *Optische und taktile Nanosensoren auf der Grundlage des Fokusverfahrens fÃ¼r die Anwendung in Nanopositionier- und Nanomessmaschinen* Dissertation. TU Ilmenau, (2012).
5. H. Baitinger, *Untersuchungen zum Einfluss der Beugung auf die Kantendetektion mit einem Autofokussensor* Diplomarbeit, TU Ilmenau, (2008).
6. P. Boher, J. Petit, L. Teroux, J. Foucher, Y. Desieres, J. Hazard, P. Chaton, *Proc. SPIE* **5752** (2005) 192-203.
7. J. Bischoff, R. Mastylo, G. Granet, E. Manske, *Proc. SPIE* **11057** (2019).
8. https://www.optocraft.de
9. S. Roy, N. Kumar, S. F. Pereira and H. P. Urbach, *J. Opt*. **15** (2013) 1-9.
10. G. Jäger, E. Manske, T. Hausotte, A. Müller, F. Balzer, *Surface Topography: Metrology Properties* **4** (2016).
11. M. G. Moharam, D. A. Pommet and E. B. Grann, *J. Opt. Soc. Am. A* **12** (1995) 1077-1086.
12. J. Bischoff, *Beiträge zur theoretischen und experimentellen Untersuchung der Lichtbeugung an mikrostrukturierten Mehrschichtsystemen*, Habilitationsschrift TU Ilmenau, (2000).
13. H. Kim, J. Park, B. Lee, *Fourier Modal Method and Ist Applications in computational Nanophotonics*, (CRC Press 2012), ISBN 9781420088380
14. G. Granet, J. Chandezon, J.P. Plumey, *J. Opt. Soc. Am. A* **18** (2001) 2102-2108.
15. J. Bischoff, *SPIE Proc*. **7272** (2009).
16. http://www.unigit.net
17. M. Pisarenco, J. Maubach, I. Setija and R. Mattheij, *J. Opt. Soc. Am. A* **27** (2010) 2423-2431.
18. J. Bischoff und K. Hehl, *Proc. SPIE* **3050** (1997) 574-585.
19. L. Li, *J. Opt. Soc. Am. A* **14** (1997) 2758-2767.
20. L. Li, *J. of Modern Optics* **40** (1993) 553-573.
21. D.W. Marquardt, *SIAM Journal of Applied Mathematics* **11** (1963) 431-441.
22. J. Kennedy, and R. C. Eberhart, *Proc IEEE International Conference on Neural Networks*, Piscataway, NJ (1995) 1942-1948.
23. J. Han, *Automatisierte Parametersuche bei der Messung von Mikrostrukturen mit einem Laserfokussensor*, Master Thesis, TU Ilmenau, (2019).
24. J. Bischoff, R. Mastylo, and E. Manske, *Proc. SPIE* 10330 (2017).
25. http://www.simetrics.de/pdf/RS-N.pdf